ADVANCED FUNCTIONAL MATERIALS

Supporting Information

for *Adv. Funct. Mater.,* DOI: 10.1002/adfm.202100205

Highly Efficient 1D/3D Ferroelectric Perovskite Solar Cell

Haijuan Zhang, Zejiao Shi, Laigui Hu, Yuan-Yuan Tang, Zhengyuan Qin, Wei-Qiang Liao, Zi Shuai Wang, Jiajun Qin, Xiaoguo Li, Haoliang Wang, Meenakshi Gusain, Fengcai Liu, Yiyi Pan, Mingsheng Xu, Jiao Wang, Ran Liu, Chunfeng Zhang, Ren-Gen Xiong, Wei E. I. Sha,* and Yiqiang Zhan**

Highly efficient 1D/3D ferroelectric perovskite solar cell

Haijuan Zhang[1]*, Zejiao Shi[1]*, Laigui Hu[1]*, Yuan-Yuan Tang[3], Zhengyuan Qin[4], Wei-Qiang Liao[3], Zi Shuai Wang[5], Jiajun Qin[1], Xiaoguo, Li[1], Haoliang Wang[1], Meenakshi Gusain[1], Fengcai liu[1], Yiyi Pan[1], Mingsheng Xu[1], Jiao Wang[1], Ran Liu[1], Chunfeng Zhang[4], Ren-Gen Xiong[2, 3]†, Wei E.I. Sha[6]†, Yiqiang Zhan[1]†

1. Center for Micro Nano Systems, School of Information Science and Technology (SIST), Fudan University, Shanghai 200433, P. R. China

2. Jiangsu Key Laboratory for Science and Applications of Molecular Ferroelectrics, Southeast University, Nanjing 211189, P. R. China.

3. Ordered Matter Science Research Center, Nanchang University, Nanchang 330031, P. R. China

4. National Laboratory of Solid State Microstructures, School of Physics, and Collaborative Innovation Center for Advanced Microstructures Nanjing University, Nanjing 210093, P. R. China.

5. Department of Electrical and Electronic Engineering, The University of Hong Kong, Pokfulam Road, Hong Kong, P.R. China

6. State Key Laboratory of Modern Optical Instrumentation, College of Information Science and Electronic Engineering, Zhejiang University, Hangzhou 310027, P.R. China

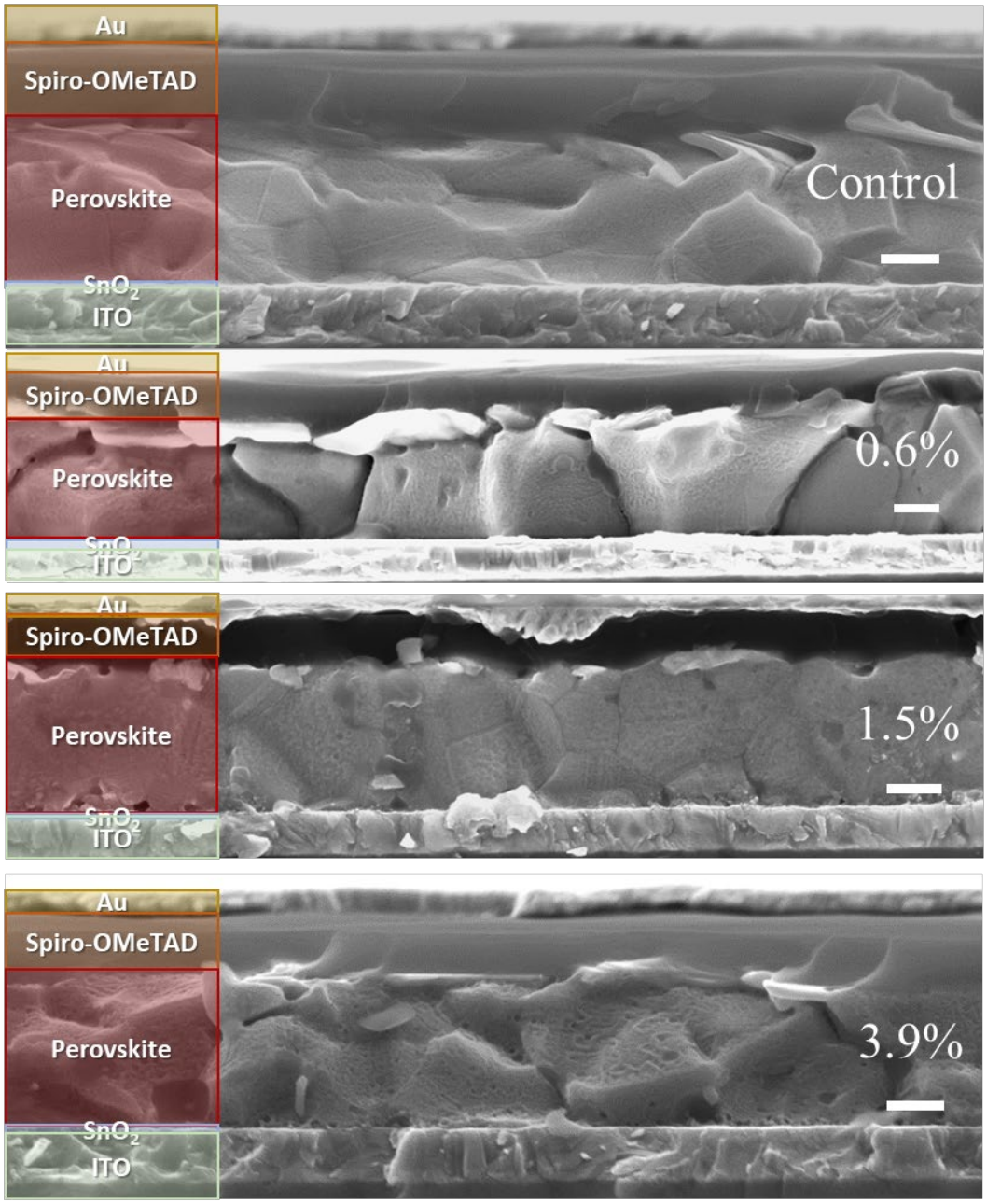

Figure S1. SEM cross section images of the control and different molar ratios 1D/3D mixed OIHP films. Scale bar: 0.2 μm. The thickness of perovskite layer is around 500 nm.

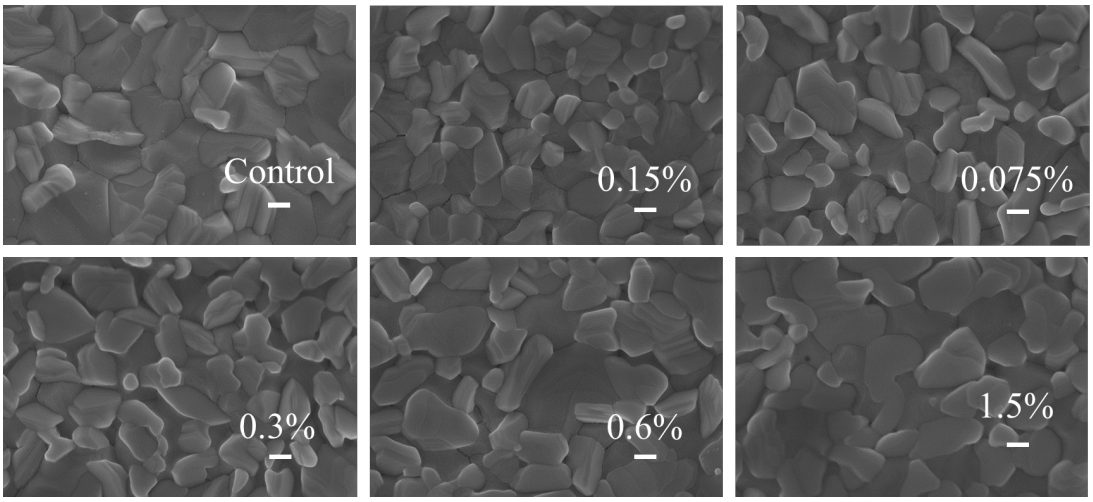

Figure S2. Top-view SEM images of the control and different mol ratios 1D/3D mixed OIHP films. Scale bar: 0.2 μm.

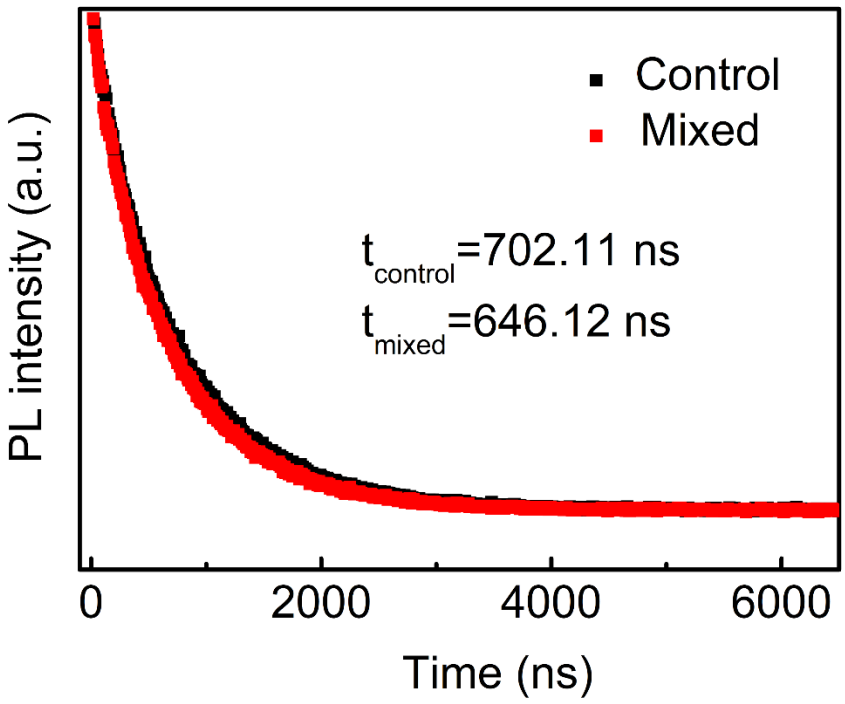

Figure S3. TRPL spectra of control and 1D/3D mixed OIHP films.

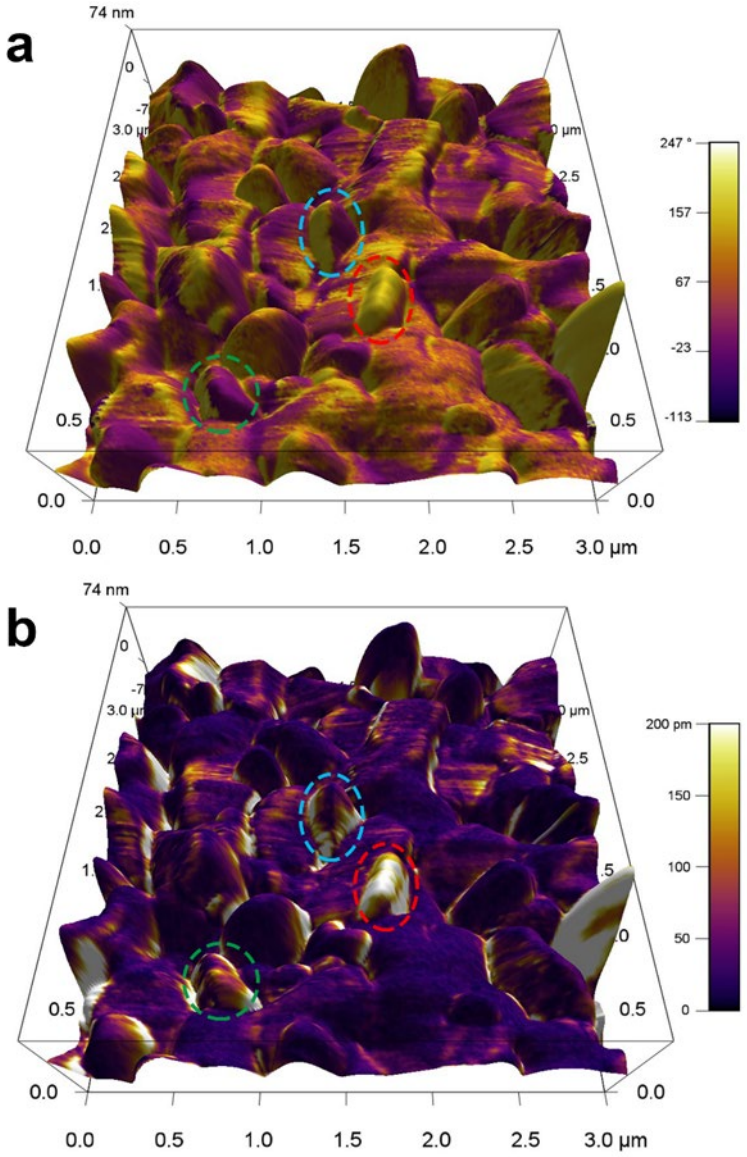

Figure S4. Phase mapping (a) and amplitude mapping (b) of the lateral PFM overlaid on the 3D topography for the thin film (1D/3D mixed OIHP). It is clear that the piezoresponse has no obvious correlation with the local topology of the sample surface. We chose three areas marked with dotted ellipses of different colors for detailed explanation. From the phase and amplitude images, we can see that the domain walls are not only at the highest boundary of the grain, but also at the left and right of the grains. Moreover, the adjacent domains on either side of domain walls have nearly equal amplitude signals, rather than that high amplitude signals occur on the same side of the grain. These results indicate there is no significant correlation between the contrast in both amplitude and phase images and the scan direction of the cantilever.

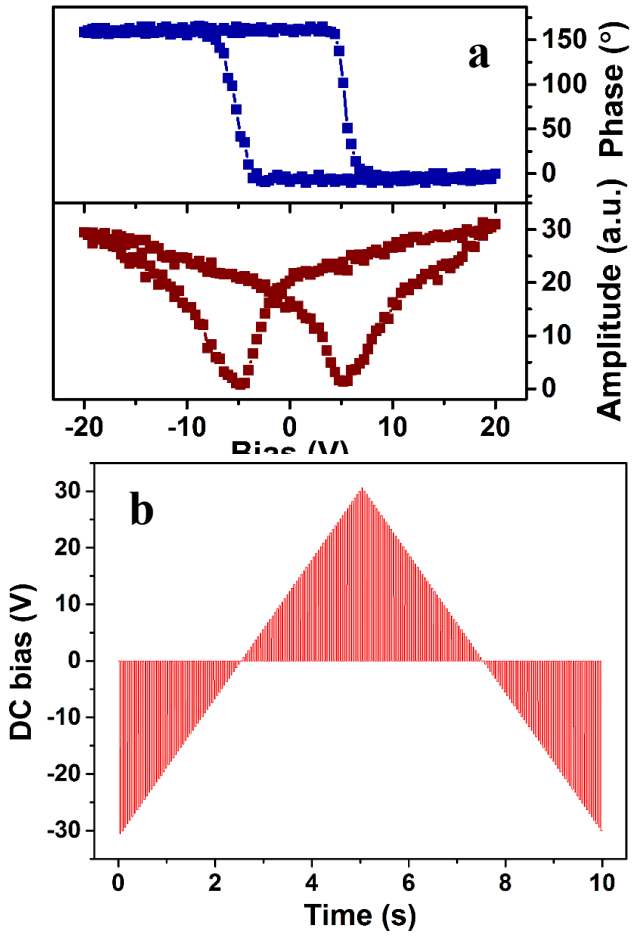

Figure S5. (a). Dependence of phase and amplitude signals with applied DC bias for a selected point on the 1.1 μm thin film (1D/3D mixed OIHP) on the ITO substrate when the sample is grounded, showing a hysteresis loop and a butterfly curve. The local coercive voltage is about 5 V, as indicated by the minima of the amplitude loop.

(b). In the hysteresis measurement shown in Figures. 2d and S5, an AC drive voltage is carried by a stepped DC bias voltage during the switching process. In order to minimized the electrostatic effect, the piezoresponse induced by V_{AC} is recorded after each step when V_{DC} = 0.

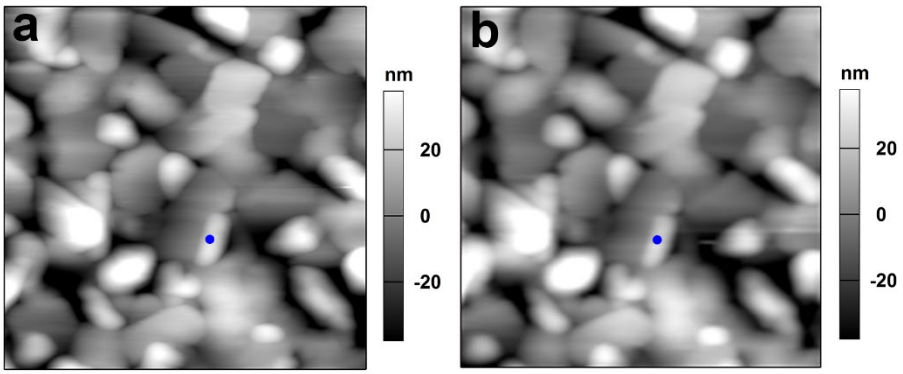

Figure S6. Topographic images of the thin film (1D/3D mixed OIHP) before (a) and after (b) the measurement of the hysteresis. The blue points indicate where the DC-sweep shown in Figure 2d was performed.

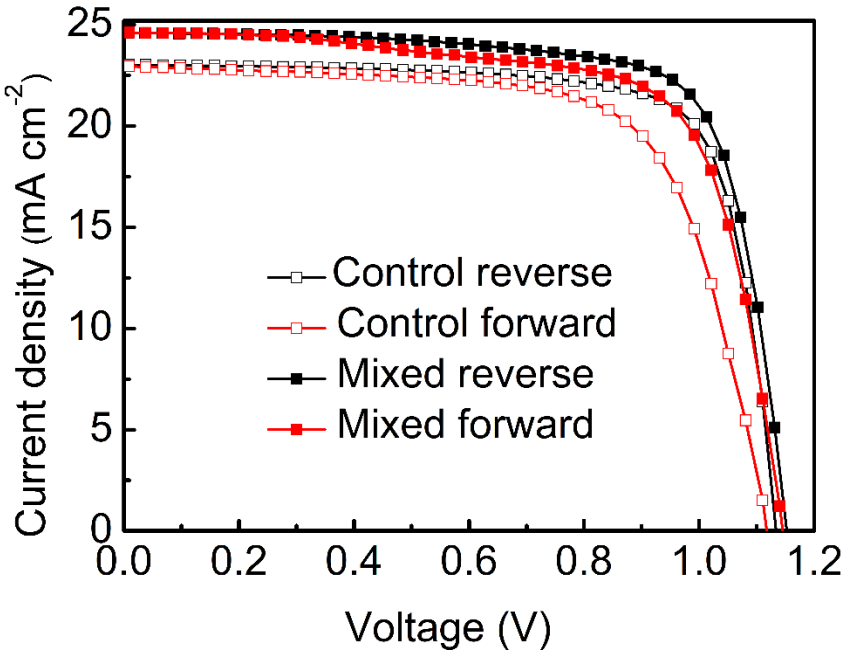

Figure S7. *J–V* curve obtained by reverse scan and forward scan for the control and 1D/3D mixed OIHP solar cell.

Table S1. J_{sc}, V_{oc}, *FF* ,*PCE* and Hysteresis parameters of control and 1D/3D mixed OIHP solar cell.

	J_{sc} (mA cm^{-2})	V_{oc} (V)	FF (%)	PCE (%)	Hysteresis Index
Control reverse	23.1	1.13	77	20.1	11.9%
Control forward	22.9	1.12	69	17.7	
Mixed reverse	24.6	1.15	75	21.2	5.2%
Mixed forward	24.6	1.15	71	20.1	

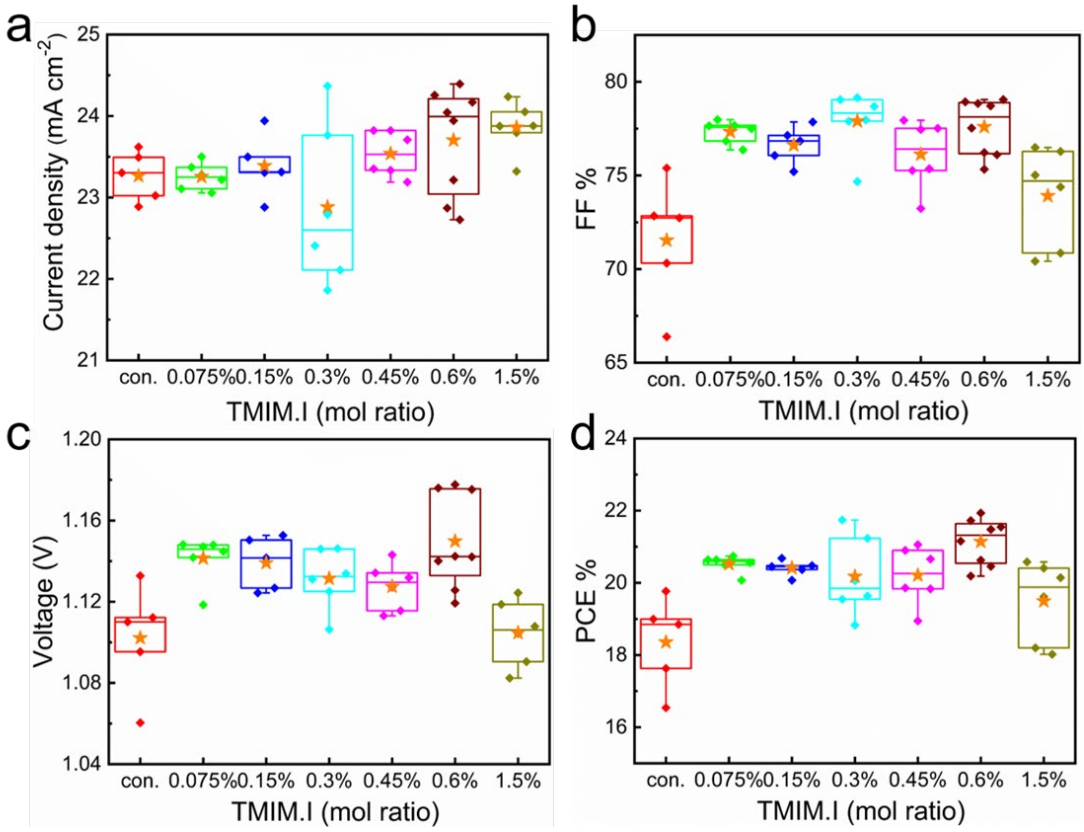

Figure S8. Statistics of J_{sc}, V_{oc}, *FF* and *PCE* parameters of control and different molar ratios of 1D perovskite phase in the 1D/3D mixed OIHP solar cells before poling.

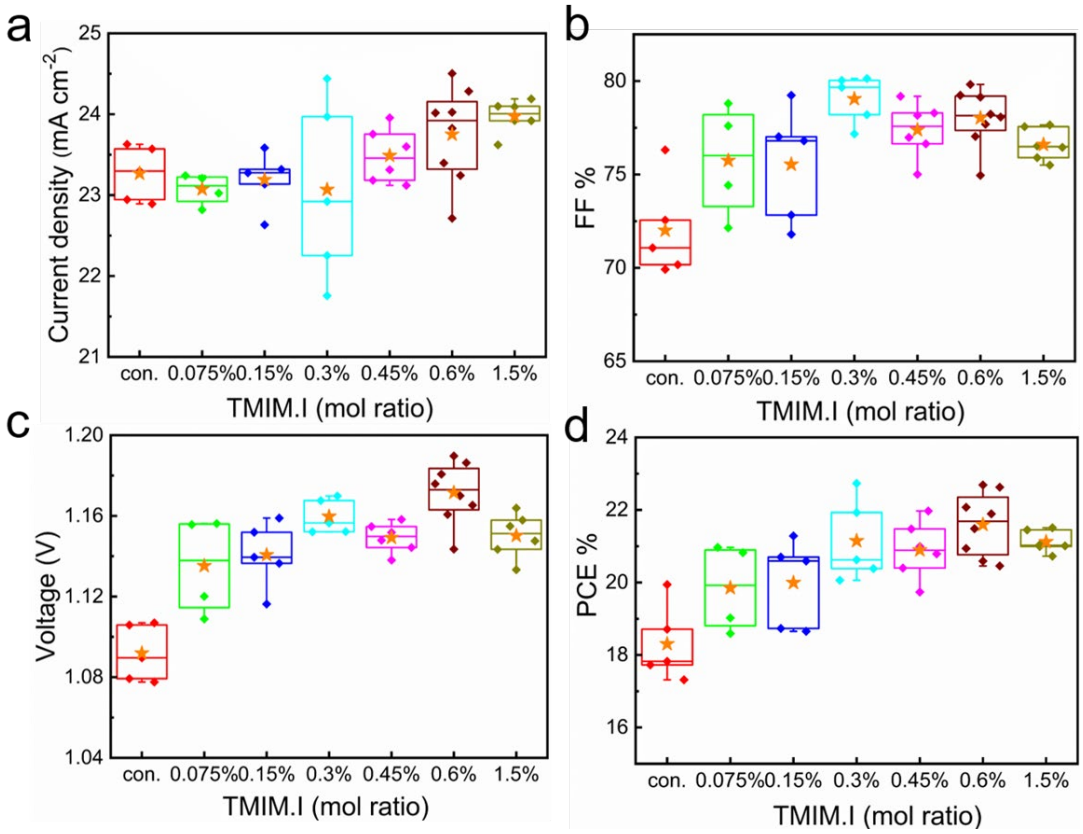

Figure S9. Statistics of J_{sc}, V_{oc}, *FF* and *PCE* parameters of control and different molar ratios of 1D perovskite phase in the 1D/3D mixed OIHP solar cells after poling.

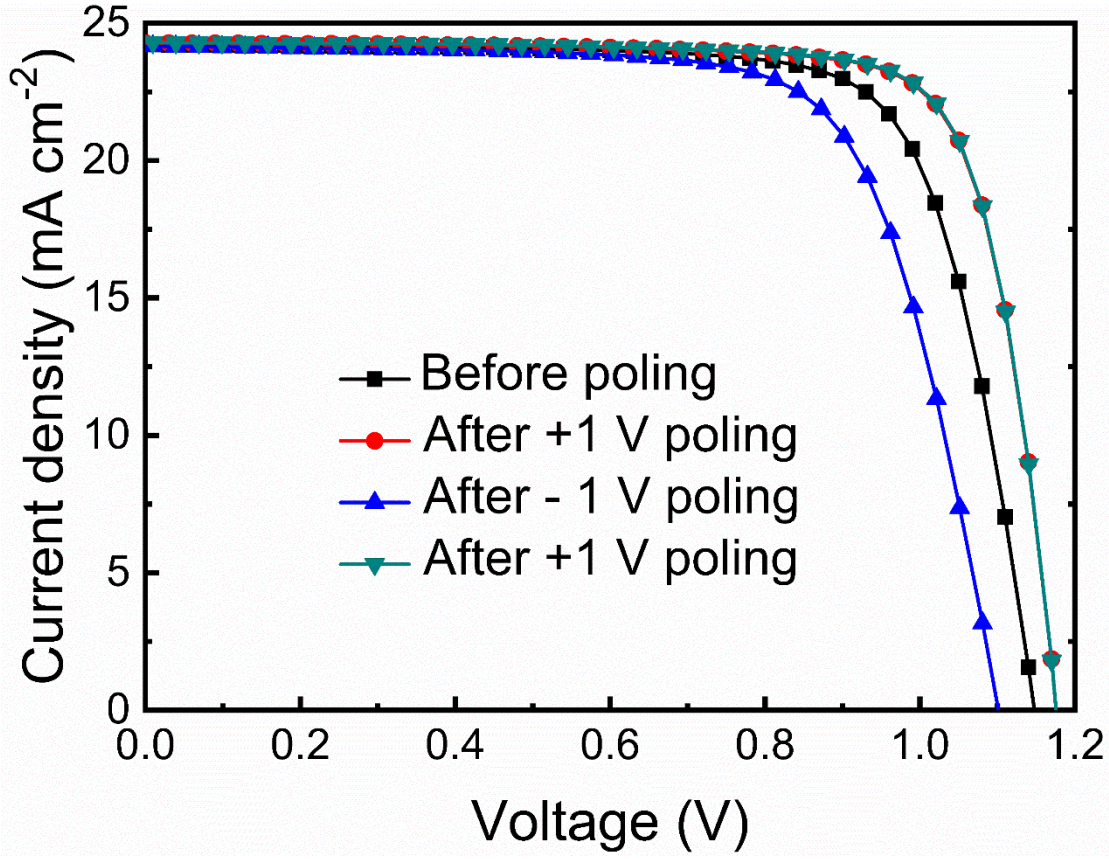

Figure S10. *J-V* curves of 1D/3D mixed OIHP solar cells before and after repeated poling.

Table S2. J_{sc}, V_{oc}, *FF* and *PCE* parameters of above 1D/3D mixed OIHP solar cells before and after poling.

	J_{sc} (mA cm^{-2})	V_{oc} (V)	FF (%)	PCE (%)
Before poling	24.2	1.15	75	21.0
After 1V poling	24.3	1.18	79	22.6
After -1V poling	24.2	1.10	72	19.1
After 1V poling	24.3	1.18	79	22.6

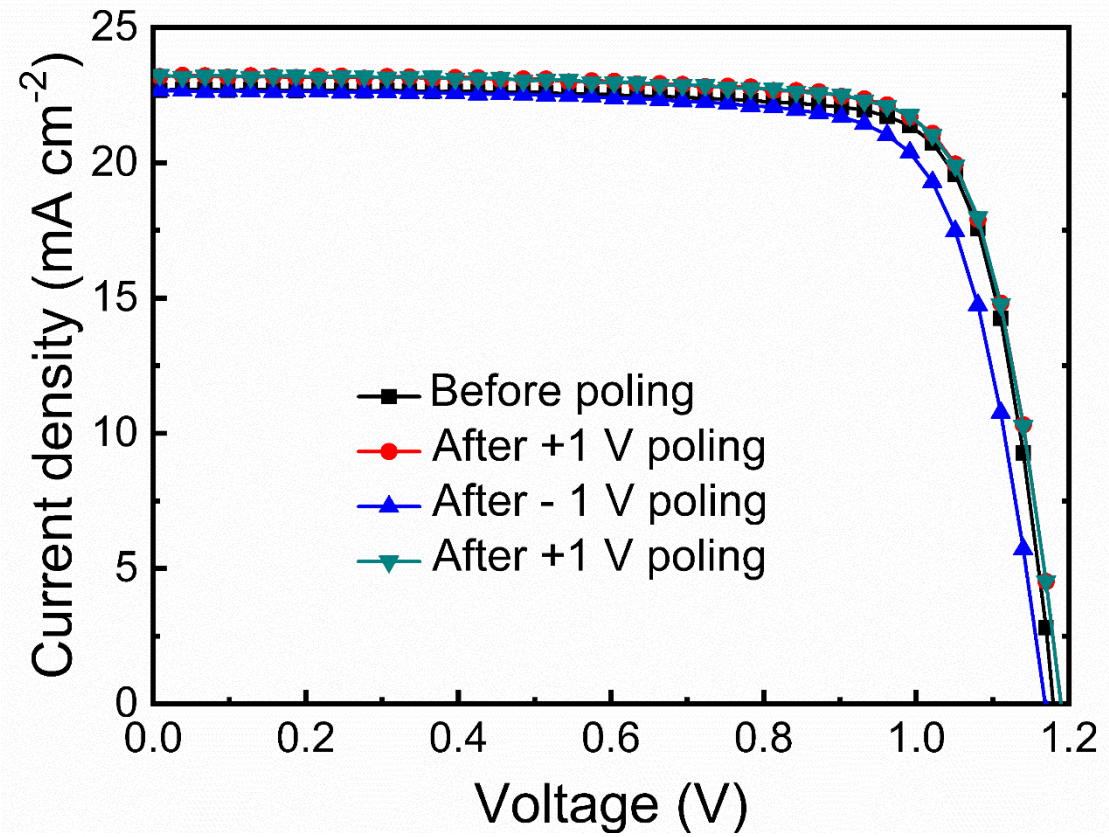

Figure S11. *J-V* curves of the champion Voc (1.19 V) for 1D/3D hybrid perovskite solar cells before and after repeated poling.

Table S3. J_{sc}, V_{oc}, *FF* and *PCE* parameters of above 1D/3D mixed OIHP solar cells before and after poling.

	J_{sc} (mA cm^{-2})	V_{oc} (V)	FF (%)	PCE (%)
Before poling	22.7	1.18	79	21.2
After 1 V poling	23.2	1.19	78	21.6
After -1 V poling	22.7	1.17	76	20.2
After 1 V poling	23.2	1.19	78	21.6

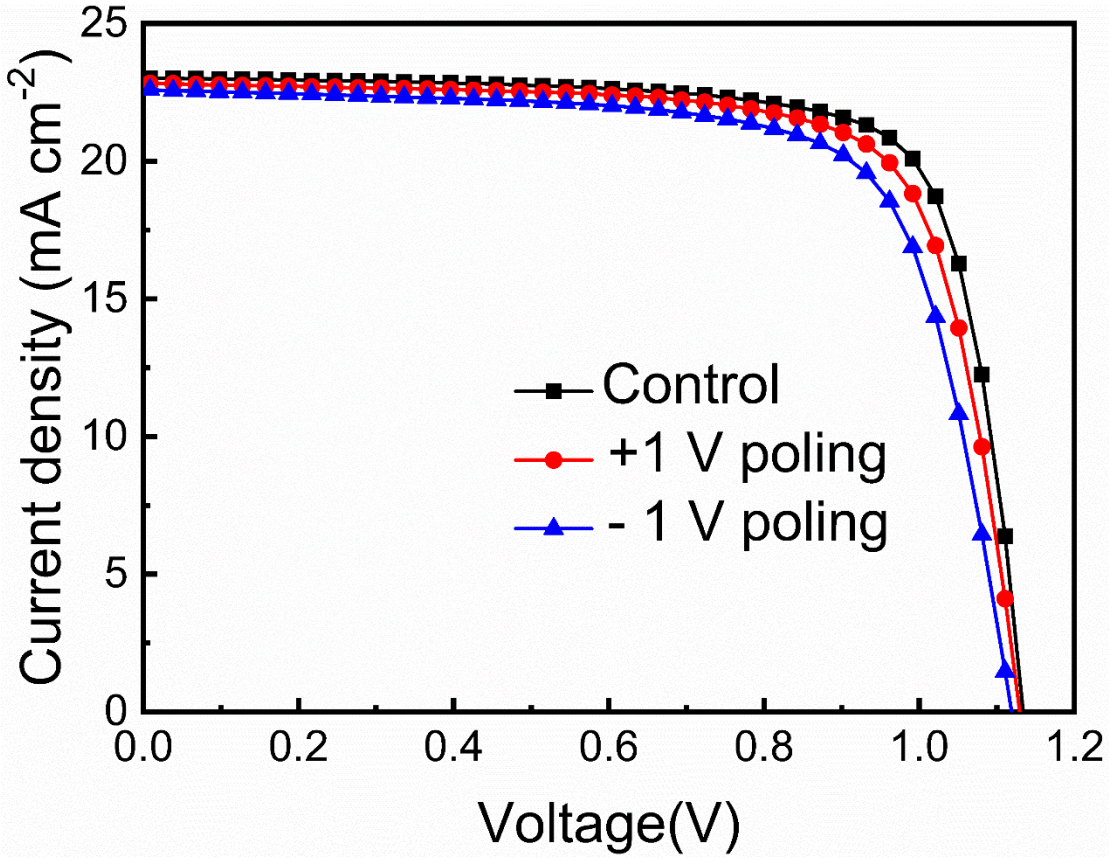

Figure S12. *J-V* curves of control OIHP solar cells before and after poling.

Table S4. J_{sc}, V_{oc}, *FF* and *PCE* parameters of the above control OIHP solar cells before and after poling.

	J_{sc} (mA cm^{-2})	V_{oc} (V)	FF (%)	PCE (%)
Before poling	23.0	1.13	77	20.1
After 1V poling	22.8	1.13	75	19.2
After -1V poling	22.6	1.12	72	18.2

The coercive field

To quantitively compare the coercive field in the device and in the PFM is not very easy. As the structures of devices and the thicknesses of perovskite films are both different. In the solar cells, there are the ETL and HTL in the device, and the thickness of perovskite is around 500 nm. The perovskite film for PFM measurement are directly deposited on ITO, with no ETL and HTL, and the thickness is over 1 μm. Furthermore, the shape of electric field in solar cells is different as the one in the PMF measurement, which might influence the coercive field as well.

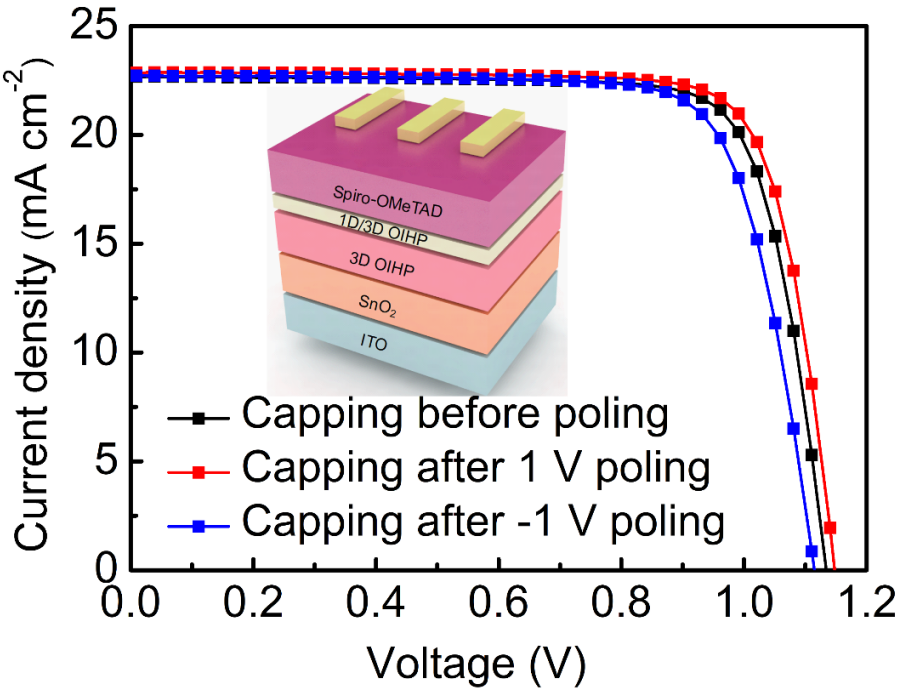

Figure S13. *J-V* curves of capping OIHP solar cells before and after poling.

Table S5. J_{sc}, V_{oc}, *FF* and *PCE* parameters of above capping OIHP solar cells before and after poling.

	J_{sc} (mA cm^{-2})	V_{oc} (V)	FF (%)	PCE (%)
Before poling	22.8	1.13	79	20.3
After 1 V poling	22.8	1.15	80	20.9
After -1 V poling	22.7	1.11	77	19.5

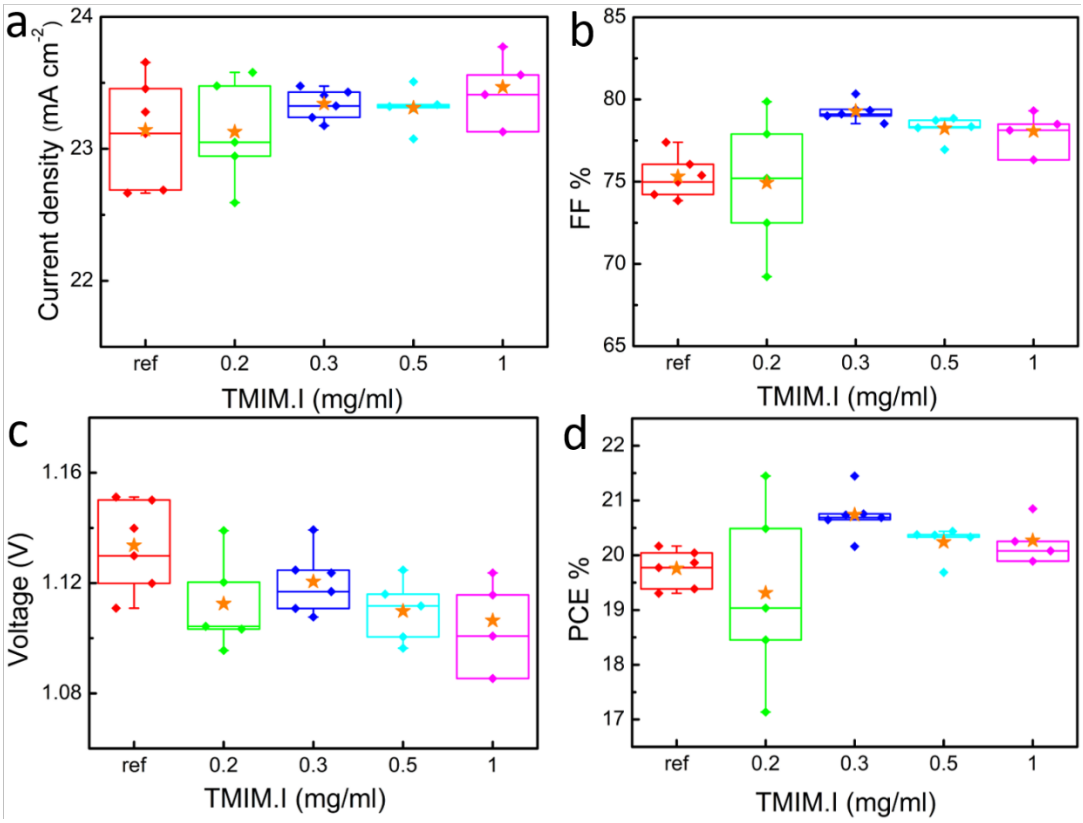

Figure S14. Statistics of J_{sc}, V_{oc}, *FF* and *PCE* parameters of control and different concentrations 1D/3D capping OIHP solar cells before poling.

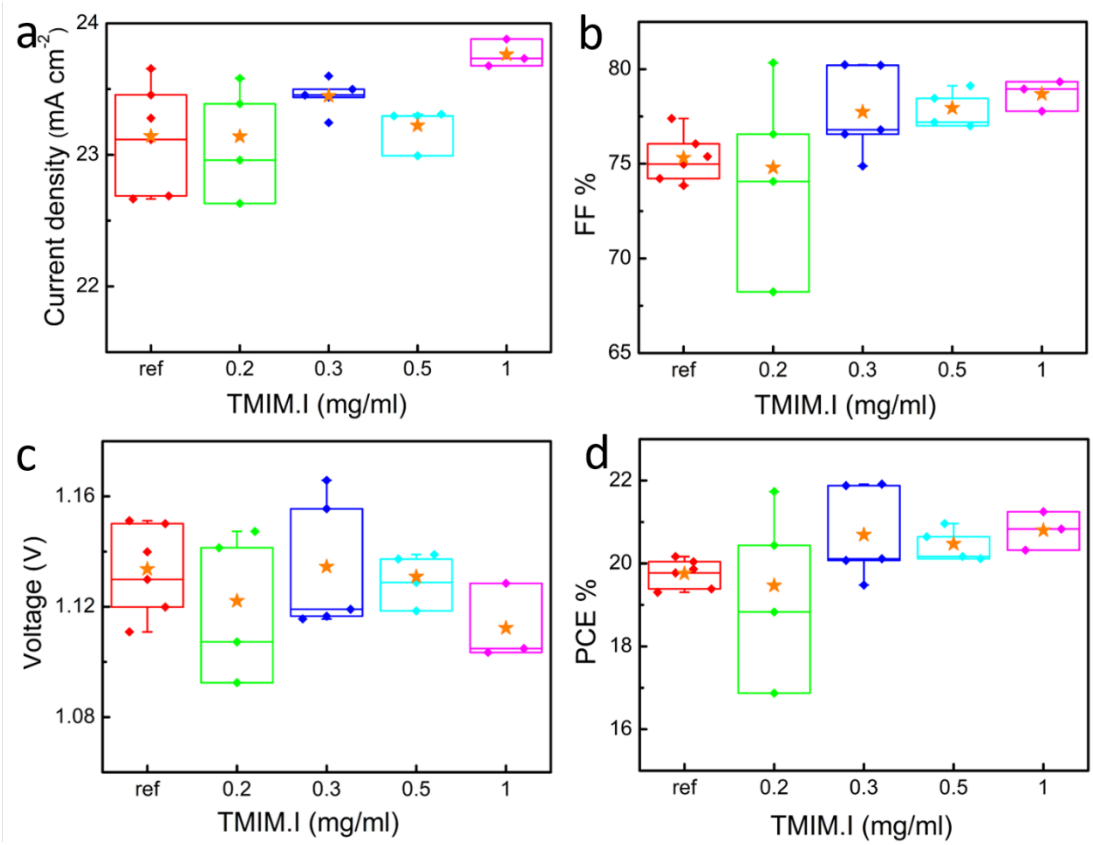

Figure S15. Statistics of J_{sc}, V_{oc}, *FF* and *PCE* parameters of control and different concentrations 1D/3D capping OIHP solar cells after poling.

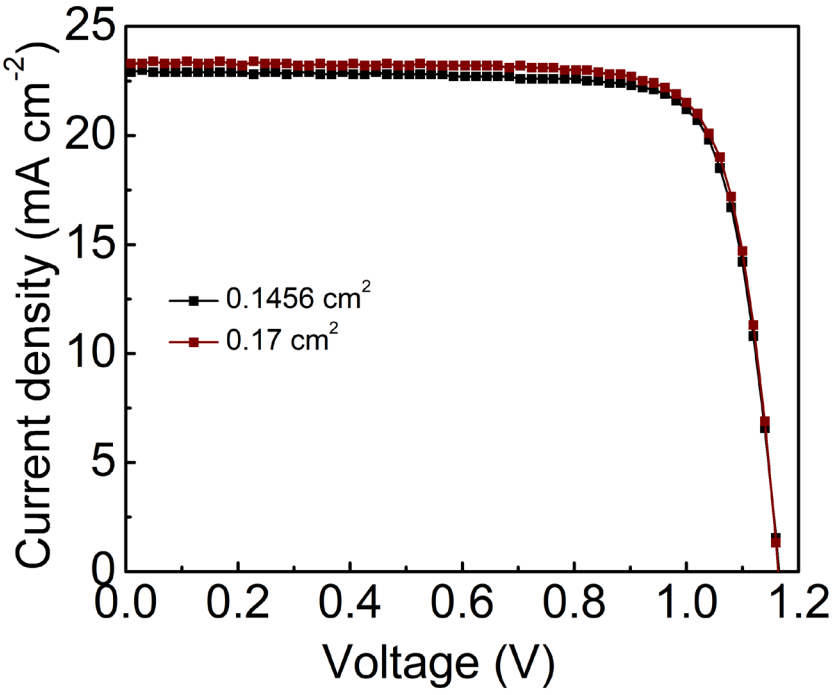

Figure S16. *J-V* characters of 1D/3D mixed OIHP solar cells after poling with (0.1456 cm^{-2}) and w/o (0.17cm^{-2}) aperture during testing.

Table S6. J_{sc}, V_{oc}, *FF* and *PCE* parameters of 1D/3D mixed OIHP solar cells after poling with (0.1456 cm^{-2}) and w/o (0.17cm^{-2}) aperture during testing.

Area (cm^2)	J_{sc} (mA cm^{-2})	V_{oc} (V)	FF (%)	PCE (%)
0.1456	22.9	1.17	80	21.3
0.17	23.3	1.16	79	21.6

Capacitance characteristics

A layer of 1D and 3D mixed perovskite film was deposited on the aluminum splitter finger electrode. The channel width of the split-finger electrode is 10 μm. The capacitance of 1D/3D mixed perovskite device before poling was measured under dark condition, with different frequency. And then the 1D/3D mixed perovskite device is polarized for 70 s at 18 V, which gives similar electric field as on the vertical device. The capacitance of the polarized 1D/3D mixed perovskite device was measured under the same condition. For the comparison, a control device with 3D perovskite and same structure are fabricated and measured. The results are shown in Figure S17.

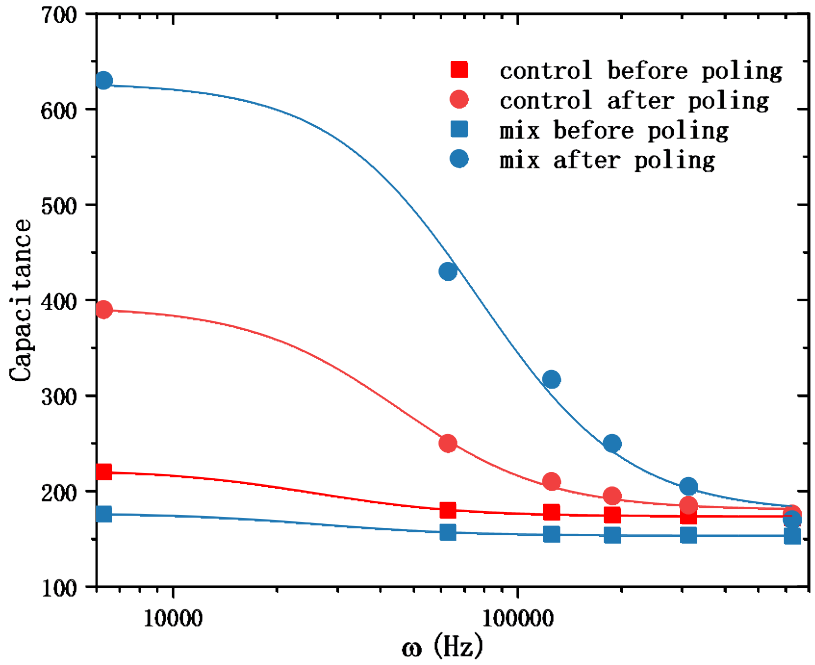

Figure S17. Capacitance measurement results and corresponding Debye models fitted for the control device and 1D/3D mixed device before and after poling. The Debye model is given by $C = C_0 \frac{\epsilon_s + \omega^2\tau^2\epsilon_\infty}{1+\omega^2\tau^2}$, where ϵ_s and ϵ_∞ are the static and high-frequency dielectric constants, respectively. τ is the relaxation time. ω is the angular frequency. The relationship between the angular frequency ω and the frequency f is: ω = 2 π f.

Table S7. Fitted Debye models for the control device and 1D/3D mixed device before and after poling.

	control before poling	**control after poling**	**mix before poling**	**mix after poling**
ϵ_s	222.76±2.23	393.80±5.29	177.25±0.56	627.97±17.3
ϵ_∞	173.75±1.02	180.54±3.16	153.54±0.27	177.54±12.8
τ	3.90e-5±7.24e-6	2.22e-5± 1.40e-6	3.76e-5 ± 3.57e-6	1.30e-5 ± 1.13e-6

Drift-diffusion simulation

The drift-diffusion simulation was conducted by our home-made transient drift-diffusion model. The governing equations of this model include:

$$\frac{\partial n}{\partial t} = \frac{1}{q}\frac{\partial J_n}{\partial x} + G - R \quad \text{(S1)}$$

$$\frac{\partial p}{\partial t} = -\frac{1}{q}\frac{\partial J_p}{\partial x} + G - R \quad \text{(S2)}$$

$$\frac{\partial a}{\partial t} = -\frac{1}{q}\frac{\partial J_a}{\partial x} \quad \text{(S3)}$$

$$\frac{\partial^2 V}{\partial x^2} = -\frac{q}{\varepsilon_0 \varepsilon_r}(n - p - a + N_{static} + N_A - N_D) \quad \text{(S4)}$$

where Equations S1-S3 are the continuity equations of electron (n), hole (p), and positive mobile ion (a), and Equation S4 is the Poisson's equation. N_{static} is the negative immobile ion and N_A and N_D are the doping densities for buffer layers. G and R refer to the generation rate and recombination rate, respectively, where the generation rate used in this simulation study is uniform in the absorber and the recombination includes radiative recombination, SRH recombination, as expressed below:

$$R_{rad} = k_{rad}(np - n_{in}^2) \quad \text{(S5)}$$

$$R_{SRH} = \frac{np - n_i^2}{\tau_n(p + p_t) + \tau_p(n + n_t)} \quad \text{(S6)}$$

Capture cross-section and density of the trap are represented by the reciprocal of their product, SRH lifetime $\tau_{n(p)}$, which is more intuitional and directly related to the lifetime measured in transient photoluminescence study. If the surface recombination is needed in the simulation study, the defect-assisted surface recombination will be set into SRH type as:

$$R_{surf} = \frac{n^+ p^- - n_i^2}{\tau_{surfn}(p^- + p_t) + \tau_{surfp}(n^+ + n_t)} \quad \text{(S7)}$$

where n^+ and p^- are the electron and hole densities on the two sides of the interface, respectively, and $\tau_{surfn(p)}$ donates the surface recombination lifetime, which is physically related to the reciprocal of the product of surface defect density and its capture cross section. The surface recombination R_{surf} will be added in Eqs. S1-S2 in addition to R_{SRH}.

The drift-diffusion current terms in the continuity equations are:

$$J_n = q\mu_n\left(n\frac{d\psi_n}{dx} + k_B T\frac{dn}{dx}\right) \quad \text{(S8)}$$

$$J_p = q\mu_p\left(p\frac{d\psi_p}{dx} - k_B T\frac{dp}{dx}\right) \quad \text{(S9)}$$

$$J_a = q\mu_a\left(a\frac{dV}{dx} - k_B T\frac{da}{dx}\right) \quad \text{(S10)}$$

Carrier mobilities of electron, hole, and positive mobile ion are μ_n, μ_p, μ_a, respectively, and Einstein's relation is implicitly included. T is temperature, and k_B is Boltzmann constant. It is worth noting that the potential terms in Equations S8-

S9, $\psi_{n/p}$, and in Equation S10, V, are different, as $\psi_{n/p}$ includes the effect from the energy band structures, expressed as:

$$\psi_n = V + \frac{\chi}{q} + \frac{k_B T}{q}\ln(N_c) \qquad \text{(S11)}$$

$$\psi_p = V + \frac{\chi}{q} + \frac{E_g}{q} - \frac{k_B T}{q}\ln(N_V) \qquad \text{(S12)}$$

For continuity equations of electron and hole, current boundary conditions are applied, as:

$$J_{nc} = S_{nc}(n - n_{0c}) \qquad \text{(S13)}$$

$$J_{na} = S_{na}(n - n_{0a}) \qquad \text{(S14)}$$

$$J_{pc} = S_{pc}(p - p_{0c}) \qquad \text{(S15)}$$

$$J_{pa} = S_{pa}(p - p_{0a}) \qquad \text{(S16)}$$

where S_{nc}, S_{pa}, S_{na}, S_{pc} are surface recombination velocities, and n_{0c}, n_{0a}, p_{0c}, p_{0a} are the boundary values of electron and hole densities at the electrodes, determined by the Schottky barriers. Infinite large surface recombination velocities for majority carriers (S_{nc}, S_{pa}) and zero surface recombination velocities for minority carriers (S_{np}, S_{pc}) represent the perfectly selective contacts.

For the continuity equation of positive mobile ion, Dirichlet boundary condition is applied, indicating the contacts are insulating for ionic carriers:

$$\mathrm{a(x = 0) = a(x = d) = 0} \quad \text{(S17)}$$

where x=0 and x=d represent the spatial grids at cathode and anode, and d refers to the thickness of the device. What insulates the transport of mobile ion across the perovskite/CTL interface is the zero mobility in the CTL.

For Poisson's equation, we also apply the Dirichlet boundary condition:

$$\mathrm{V(x = 0)} = -WF_{cathode} \quad \text{(S18)}$$

$$\mathrm{V(x = d)} = V_{app} - WF_{anode} \quad \text{(S19)}$$

where $WF_{cathode/anode}$ is the work function of cathode or anode, and V_{app} is the externally applied voltage.

The continuity equations were discretized in space domain by S-G scheme [1], and in time domain by backward Euler's method. These equations were solved sequentially in Gummel's iteration and the converged solutions were obtained in each time step.

Through the post-processing of the converged solution of the proposed model at specific applied voltage, we can directly plot the potential distribution as the solution of Poisson's equation (**Figure 5**a), from which we can also calculate the electric field results (**Figure 5**d). Recombination rate distribution can be obtained from the electron and hole density distributions based on the recombination equations Eqs. S5-S7 (**Figure 5**b). By sweeping the applied voltage, we will have the evolution of current density at the electrodes and plot the J-V curves as shown in **Figure 5**c.

For simplification and approximation, symmetric modeling structures were used and the input parameters were extracted from other studies or selected in the

realistic region. The device structure of p-i-n is applied in the simulation study, where the ETL and HTL are set as perfect selective CTLs with high majority carrier mobility and low minority carrier mobility. High enough blocking energetic band offsets are also set for better selectivity, whereas the surface recombination will exist at the interfaces between the CTLs and perovskite if necessary. Carrier generation rate is uniformly distributed in the absorber with the approximated value which ensures the simulated Jsc can be compared with the experiments.

Table S8. Parameters used in the drift-diffusion simulation

Parameter Names	**Symbols [units]**	**Values**		
		ETL	**Absorber**	**HTL**
Bandgap	Eg [eV]	2.3	1.6 [2]	2.3
Thickness	L [nm]	200	500	200
Electron affinity	χ [eV]	4.1	3.8	2.8
Effective Fermi level	E0 [eV]	4.2	4.6	5.0
SRH lifetime for electron and hole	T [μs]	Inf large	1 [0.1 for surface if applicable]	Inf large
Nominal radiative recombination coefficient	k_{rad} [cm^3/s]	$1.5*10^{-10}$	$3.6*10^{-12}$	$1.5*10^{-10}$
Electron mobility	μ_n [cm^2/Vs]	20	2 [3]	0
Hole mobility	μ_p [cm^2/Vs]	0	2 [3]	20
Cation mobility	μ_a [cm^2/Vs]	0	10^{-9}	0
Initial cation density	a [$/cm^3$]	0	10^{18} [4]	0
Generation rate	G [$/m^3s$]	0	$3*10^{27}$	0
Density of state	$N_{c/v}$ [$/cm^3$]	10^{19}	10^{19}	10^{19}
Relative dielectric constant	ε_r	4	31 [5]	4
Schottky barrier	B_n, B_p [eV]	0.1	--	0.1

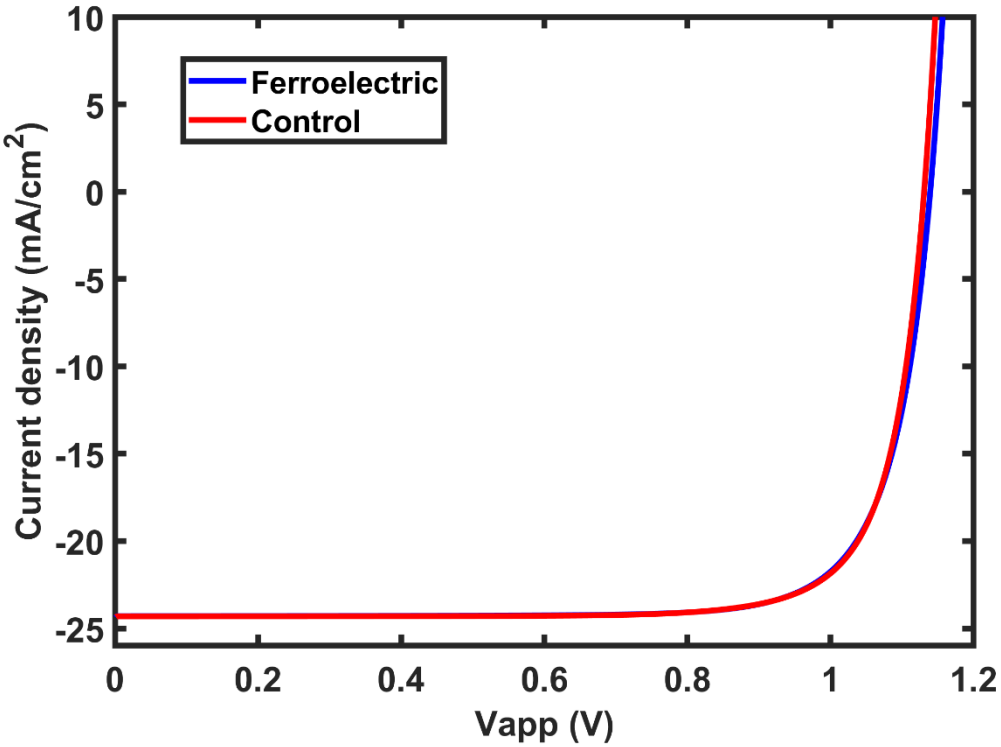

Figure S18. Compare of simulated *J-V* curves of control and ferroelectric PSCs with negligible interfacial recombination.

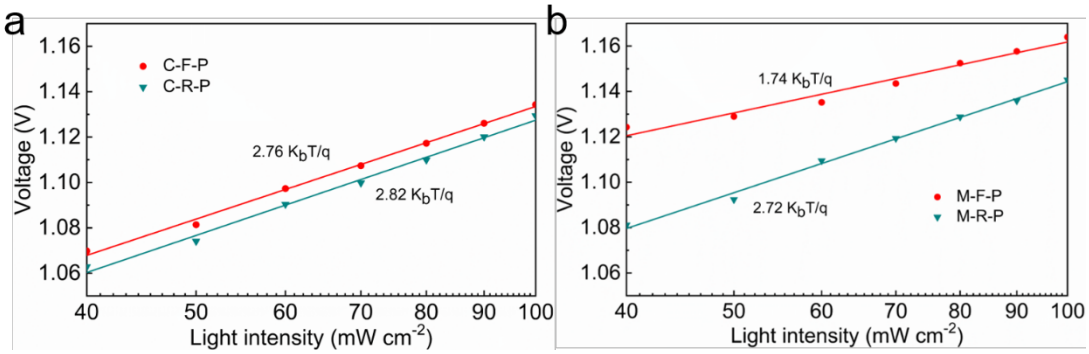

Figure S19. (a) V_{oc} versus light intensity for control PSCs with positive and negative poling. C-F-P: Control PSCs forward poling. C-R-P: Control PSCs reverse poling. (b) V_{oc} versus light intensity for 1D/3D mixed PSCs with positive and negative poling. M-F-P: Mixed PSCs forward poling. M-R-P: Mixed PSCs reverse poling. The lines in the figure are guide for the eye.

The fitting curves was performed via using the Equation (2),

$$V_{oc} = (nK_{\mathrm{B}}Tq^{-1})\ln(J_{sc}/J_0 + 1) \quad (2)$$

where n is the ideal factor, K_B is Boltzmann constant, T is temperature, q is elementary charge and J_0 is saturated dark current density. According J_0 is negligible compared with J_{sc} and J_{sc} is proportional to light intensity, the equation could be simplified as $V_{\mathrm{oc}} \propto nK_BT/q$. Relatively lower n value of 1.74 for 1D/3D mixed PSCs with positive poling (2.72 with negative poling), where an ideal trap-free system tend to close to 1, illustrates reduced trap-assistant recombination.

Low temperature polarization

A *J-V* characteristic before/after poling at room/low temperature of control (a) and 1D/3D mixed (b) PSCs have been studied systematically, to exclude the effect of ion migration.

The result in Figure S20a shows that there is no observable change of the *J-V* curves in control device after positive or negative polarization at 250 K. However, in ferroelectric PSCs even without ion migration, the current before and after poling will still differ much, indicating polarization field is contributed by ferroelectric property of 1D/3D mixed OIHP.

Furthermore, the zero of current indicates the zero of the total electric field. From Figure S20a, in the control device, at room temperature, the zero point changes in a very small range, generated by the mobile ions. However, in the ferroelectric device, the zero point has changed a lot more, which proves that the electric field arising from ferroelectric polarization is much higher than that from mobile ions.

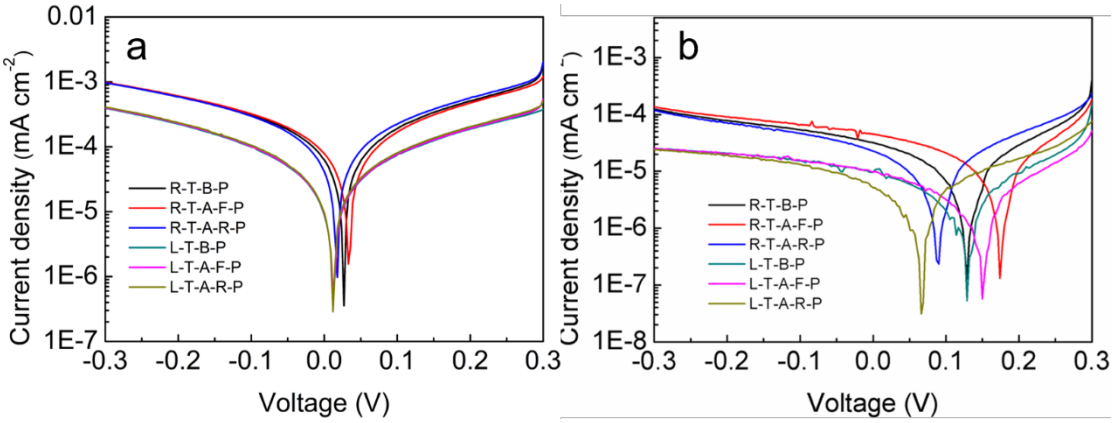

Figure S20. *J-V* characteristic before/after poling at room/low temperature of control (a) and 1D/3D mixed (b) PSCs. R-T-B-P: Room temperature before poling. R-T-A-F-P: Room temperature after forward poling. R-T-A-R-P: Room temperature after reverse poling. L-T-B-P: Low temperature before poling. L-T-A-F-P: Low temperature after forward poling. L-T-A-R-P: Low temperature after reverse poling.

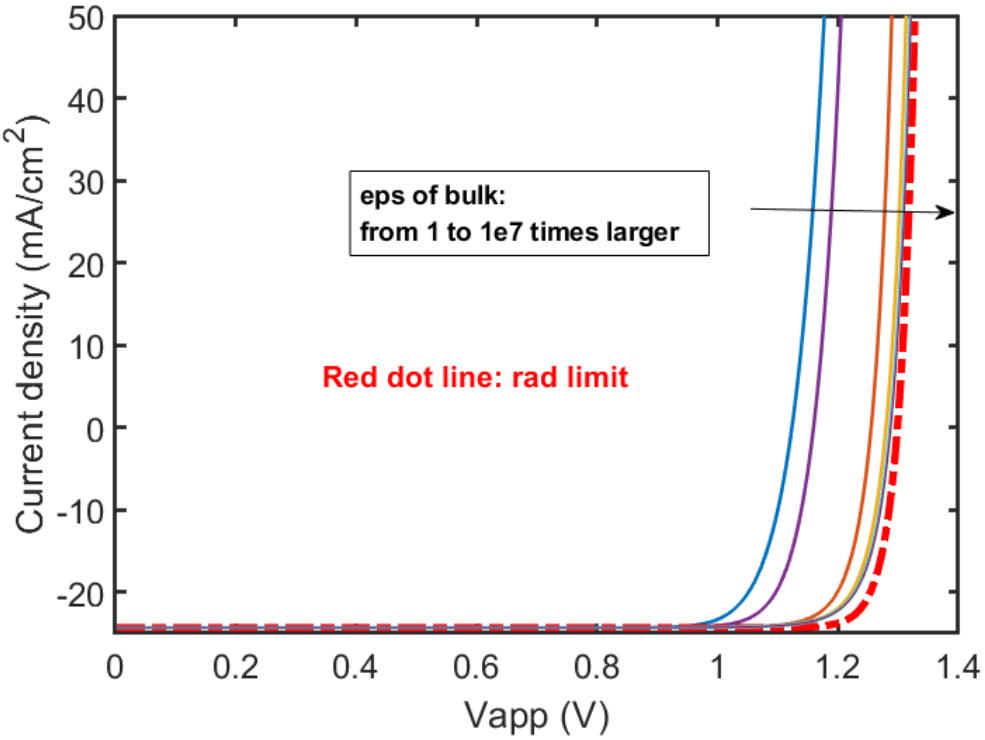

Figure S21. The simulated *J-V* characteristics of the ferroelectric PSCs with extremely large bulk dielectric constants.

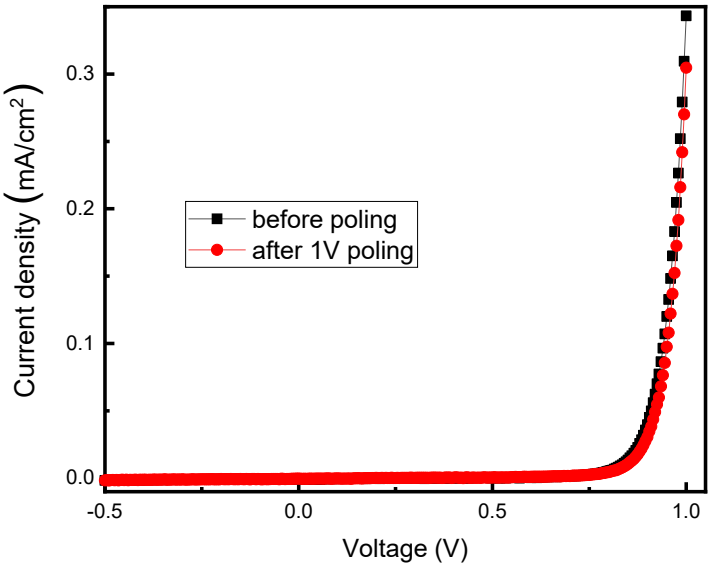

Figure S22. *J-V* curves under dark condition of 1D/3D mixed OIHP solar cell before and after poling.

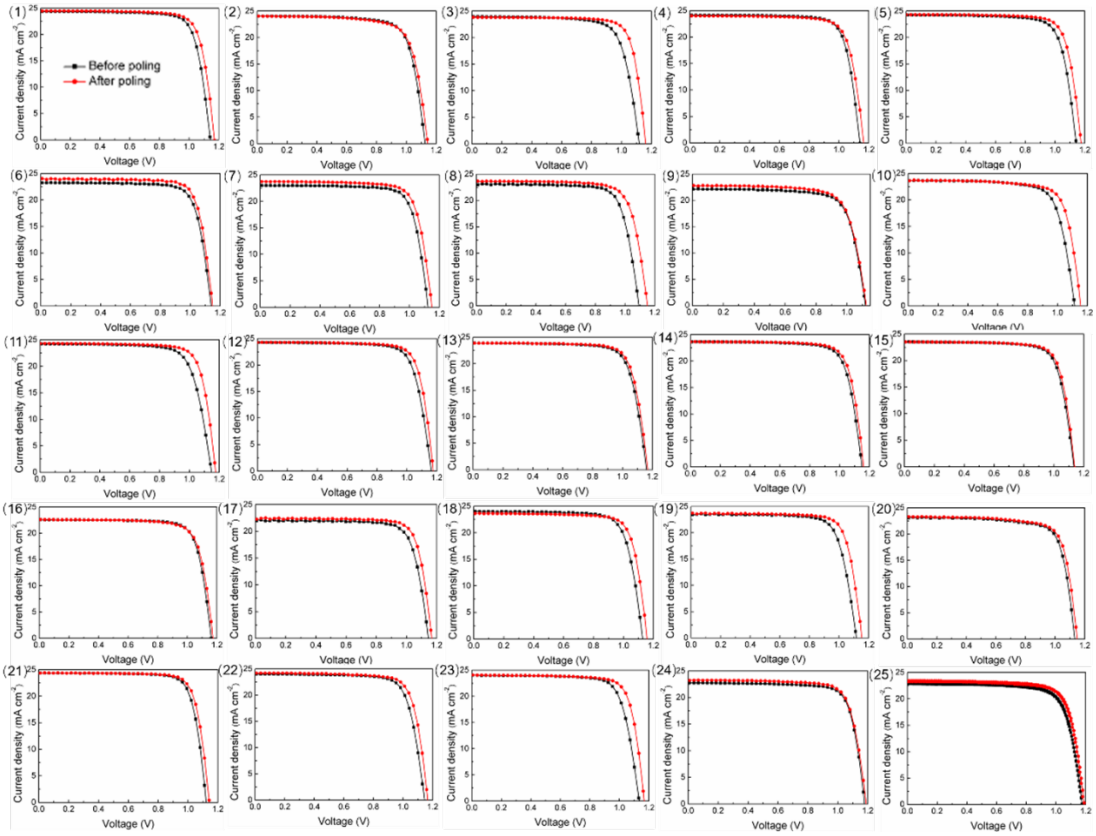

Figure S23. *J-V* curves of all 1D/3D mixed PSCs before and after poling which shown in Figure 3f.

TRPL and PL measurements

A layer of 1D/3D mixed perovskite film was deposited on the aluminum splitter finger electrode. The channel width of the split-finger electrode is 10 μm. TRPL and PL data of control device and 1D/3D mixed device were measured before and after poling. The 1D/3D mixed perovskite device is polarized for 70 s at 18 V, which gives similar electric field as on the vertical device. In the control device, there is no obvious change in TRPL or PL data. However, the PL lifetime of the 1D/3D mixed ferroelectric perovskite film is clearly increased, with a red shift of PL peak. This is a solid evidence, proving the intrinsic radiative recombination rate can be reduced by the ferroelectric polarization field.

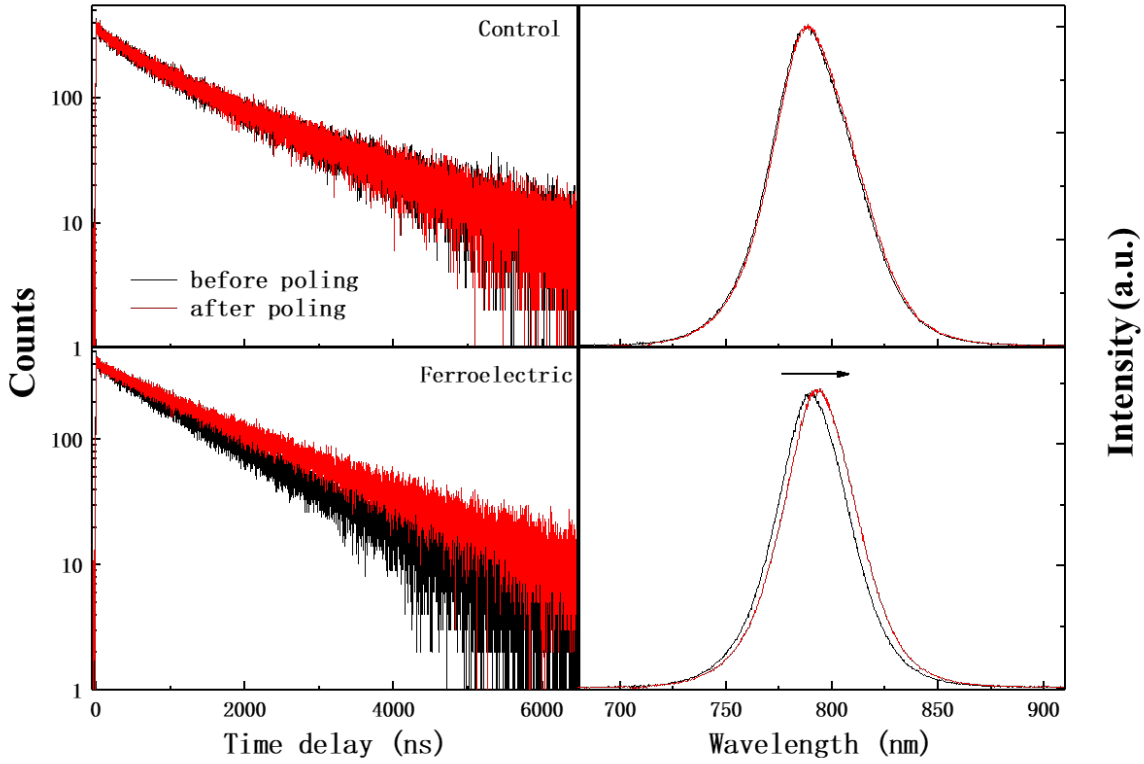

Figure S24. TRPL and PL data of control device and 1D/3D mixed device before and after poling.

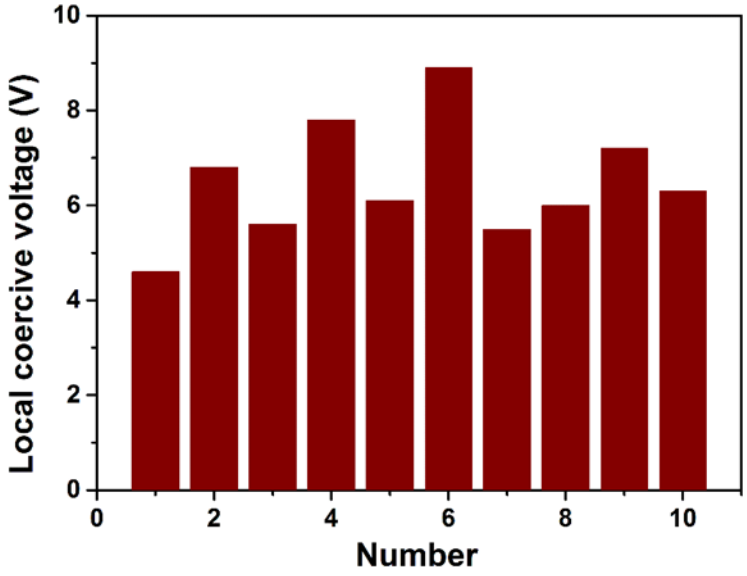

Figure S25. The local coercive voltages for ten selected points in the grains with strong amplitude signals on the thin film (1D/3D mixed OIHP) when the sample is grounded. The local coercive voltage ranges from 4.6 to 8.9 V, with an average of 6.5 V, as indicated by the minima of the amplitude loop.

We have chosen ten positions in the grains with strong amplitude signals on the 1D/3D mixed OIHP film to carry out new local PFM-based hysteresis loop measurements in the revised version. All of them can show 180° phase hysteresis loops and typical butterfly-shape amplitude loops, indicating the good reproducibility of PFM phase and amplitude switch data. Figure S1 exhibits the corresponding local coercive voltages, ranging from 4.6 to 8.9 V, with an average of 6.5 V, as indicated by the minima of the amplitude loop. For polycrystalline films, the local coercive voltages are often different in various places on a surface, due to the anisotropy of different grains.

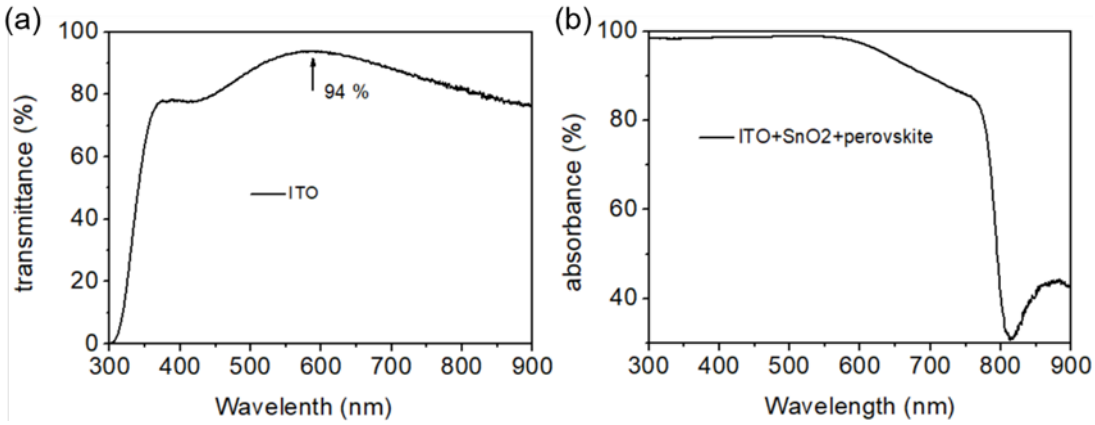

Figure. S26 (a) Transmission spectrum of ITO substrates in manuscript; (b) Absorption spectrum of ITO substrates covered with (SnO_2+ perovskite) films.

ITO with high transmittance was purchased from YiYang South China Xiangcheng Technology Co., Ltd, the product specification is "6 Ohm JM Etch". The ITO in the manuscript was used directly after purchase, without further processing. As shown in Figure S26(a), the transmittance of ITO substrate was measured, and we obtained that the light transmittance was 94% at 590 nm, which was consistent with the value provided by the company. The absorbance of the perovskite/SnO_2/ITO film was then measured, showing 98.8% at 550 nm, shown in Figure S26(b). The increase of transmittance comes from the decrease of reflection loss, as the refractive index of perovskite is much higher than ITO/glass. We agree with reviewer's suggestion to include the transmittance data as Fig S in SI.

Reference:

[1] Selberherr, Siegfried, *Analysis and simulation of semiconductor devices*, Springer-Verlag Wien, **1984**.

[2] A. M. A. Leguy, P. Azarhoosh, M. I. Alonso, M. Campoy-Quiles, P. R. F. Barnes, *Nanoscale* **2015**, *8*, 6317.

[3] T. Leijtens, S. D. Stranks, G. E. Eperon, R. Lindblad, E. M. J. Johansson, I. J. Mcpherson, H. K. Rensmo, J. M. Ball, M. M. Lee, H. J. Snaith, *ACS Nano* **2014**, *8*, 7147.

[4] A. Walsh, D. O. Scanlon, S. Chen, X. Gong, S. H. Wei, *Angew. Chem.* **2015**, *127*, 1811.

[5] M. Sendner, P. K. Nayak, D. A. Egger, S. Beck, C. Müller, B. Epding, W. Kowalsky, L. Kronik, H. J. Snaith, A. Pucci, *Mater. Horiz.* **2016**, *3*, 613.